



Contents lists available at ScienceDirect

Applied Thermal Engineering

journal homepage: www.elsevier.com/locate/apthermeng

Research Paper

Thermo-mechanical design and characterization of flexible heat pipes

Tanmay Jaipurkar^a, Pushpit Kant^a, Sameer Khandekar^{a,*}, Bishakh Bhattacharya^a, Siddharth Paralikar^b^a Department of Mechanical Engineering, Indian Institute of Technology Kanpur, Kanpur 208016, India^b Golden Star Technical Services Pvt. Ltd., Pavana Complex, A39/T204, M.I.D.C., Bhosari, Pune 411 026, India

ARTICLE INFO

Article history:

Received 27 October 2016

Revised 6 January 2017

Accepted 10 January 2017

Available online xxxx

Keywords:

Flexible wicked heat pipe

Metallic bellows

Thermal performance

Axial and radial stiffness

Design procedure

ABSTRACT

The paper describes the ongoing design, development, testing and characterization of the thermal and mechanical performance of flexible wicked heat pipes, with typical heat handling capacity of about 60 W, water as the working fluid, length of 270 mm and having internal diameters = 10 mm and 6 mm, respectively. The heat pipes are being designed for passive thermal management, wherein heat transfer is required to be coupled with vibration isolation between the evaporator and condenser sections. This prevents the heat pipe, the thermal load, and the heat sink, from getting damaged under required operating conditions. Moreover, precision positioning of thermal load/device is also maintained. The flexibility is provided in the adiabatic section of the heat pipe using a flexible metallic bellow. Experiments are performed to get the axial and angular stiffness of the used bellows and its mechanical response under static loads. A finite element model for the bellow is developed and it is benchmarked against experiments and available design equations. Successful thermal performance for heat pipes under different operating conditions, including bend configurations, is reported and bellow design procedure is outlined.

© 2017 Elsevier Ltd. All rights reserved.

1. Introduction

Heat pipes are proven passive devices which are used presently to solve a large number of thermal management problems. This technology has been successfully applied in a variety of thermal applications like heat exchangers, satellite applications, electronic cooling and economizers. Typical heat pipe works on a simple principle of phase-change phenomenon i.e. condensation and evaporation of working fluid occurring in a closed system. Heat is transferred from evaporator to condenser by utilizing latent heat of the working fluid [1–3].

The present study characterizes the thermal and mechanical performance of a flexible heat pipe. The heat pipe is made flexible using a metallic bellow element in the middle adiabatic section. The heat pipe is designed to perform heat transfer function without getting damaged under mounting and operating forces on the element/system [4–7]. The bellow element provides flexibility that prevents the heat pipe, the heat source, and the condenser/radiator from getting damaged [8,9]. Hence, other than thermal design of the heat pipe, mechanical design of the flexible element must also be performed. Haringx [10] modeled the bellow as the combination of annular plates connected by elastic cylinders and derived an expression relating the Flexural rigidity (EI) of the bellow with

geometric parameters. Haringx utilized the results of bending of flat rings which were earlier studied by Reissner [11]. Newland [12] further gave the expression relating EI to axial stiffness of bellow. In the present work, the flexible SS bellow is tested for deformations under hydrostatic pressure. The angular and axial stiffness is also measured experimentally and verified with the EJMA (Expansion Joint Manufacturing Association) standards and other available models. The heat pipe is developed for maximum heat carrying capacity of about 50 W and operating temperature range of 10–100 °C.

2. Manufacturing of heat pipe

The developed heat pipes have a flexible structure, a metallic bellow, which is attached to metal pipes made of copper, as shown in Fig. 1(a), such that the heat pipes can be bent or gets bent if external loads are experienced. The pipes have a woven screen mesh made of phosphor bronze. The mesh bents together with the heat pipe without any risk of being broken; the mesh remains in contact with the internal wall of the copper pipes and the bellow [13,14]. This is necessary to allow the working fluid to flow smoothly in the woven mesh and to maintain a good heat dissipating effect. A stainless steel bellow is used as the flexible element, cut section of which is shown in Fig. 1(b). It provides flexibility during operation and deals with axial, radial, lateral, and angular displacements. In the present study, we used EJMA standards to

* Corresponding author.

E-mail address: samkhan@iitk.ac.in (S. Khandekar).

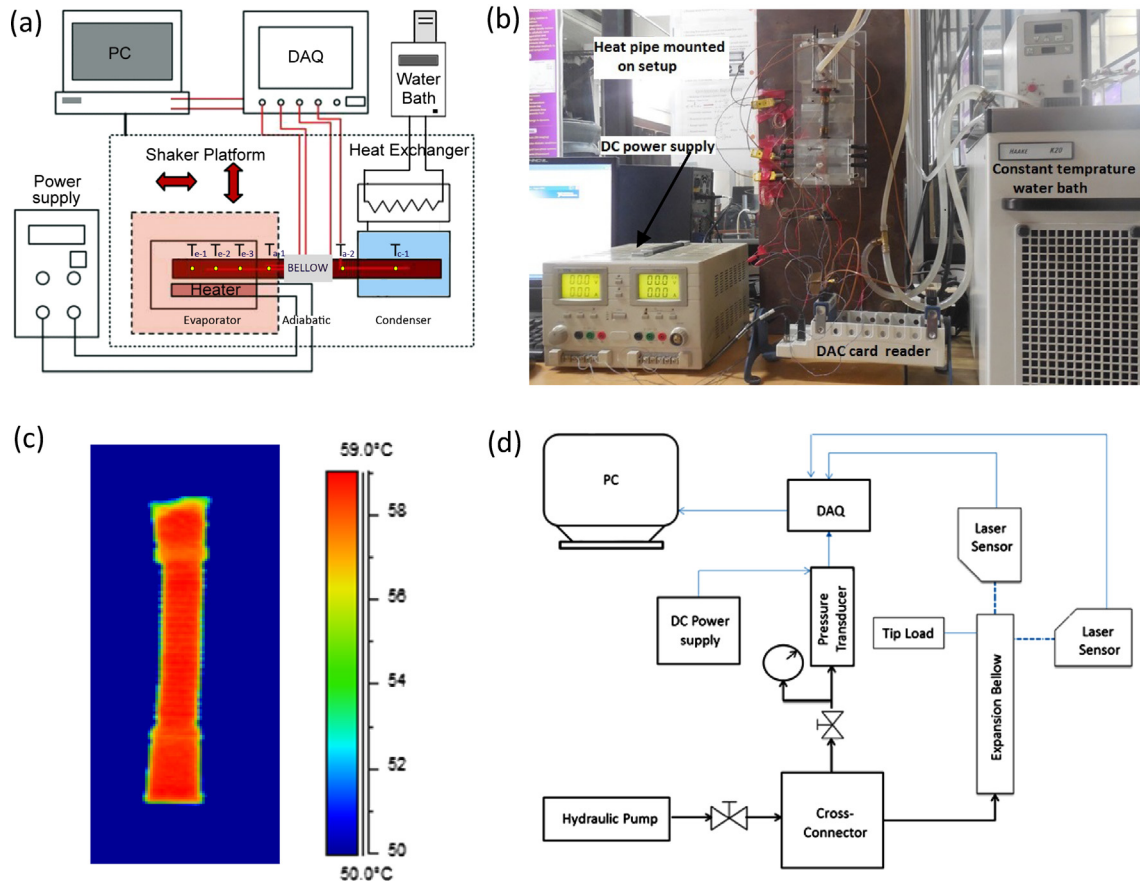


Fig. 2. Schematic details of the test setup (a) test bench used for thermal characterization of heat pipe (b) photograph of the experimental test bench (c) representative infrared thermography image of the bellow section under testing, 10 mm ID heat pipe, 10° bent position, 60 W heat input (d) schematic of test setup for pressure testing of bellow using laser sensors, pressure transducer and pressure gauge.

pipe. These deformations are measured using two laser sensors (Micro-Epsilon®), one placed in the radial direction and the other along the axis of the bellow. A cross connector is used to connect an absolute pressure transducer (Honeywell®), hydraulic pump and the bellow. Synchronized data are collected from the transducer and the laser sensors via a DAQ reader to get applied pressure v/s bellow deformation graph. The load is applied in discrete values and the resulting vertical displacements are measured using the laser sensor, placed in the perpendicular direction to the longitudinal axis of the bellow. Data are collected from the laser sensors via a DAQ reader to get applied load v/s bellow deformation graph.

3.3. Methodology and data reduction

Experiments are carried out to calculate the thermal resistance of heat pipes between the evaporator-adiabatic section and the evaporator-condenser section, in straight and deformed configurations, respectively, to characterize the performance of heat pipes in the desired operating range. Proper insulation is applied in the adiabatic/bellow section of the heat pipes to prevent heat losses. Power input is increased in steps, both in the forward and reverse directions and equilibrium condition is allowed to reach in each case. All experiments reported here are repeated, at least, three times. The thermal resistance of a heat pipe is calculated for evaporator-adiabatic and evaporator-condenser as:

$$R_{adb} = \frac{\bar{T}_{evp} - \bar{T}_{adb}}{\dot{Q}} \quad (1)$$

$$R_{cond} = \frac{\bar{T}_{evp} - \bar{T}_{cond}}{\dot{Q}} \quad (2)$$

4. Results and discussion

Figs. 3 and 4 show the thermal resistance at different power inputs for gravity assisted vertical orientation (evaporator down) and for horizontal orientation of heat pipes. The heat pipes are tested in both straight and deformed (bent) configurations of 10°. The coolant temperature is always kept at 25 °C.

4.1. Heat pipe of ID 10 mm

Fig. 3(a) shows the thermal resistance for 10 mm internal diameter heat pipe in the vertical (heater down) orientation (the dimensions of the heat pipe are given in the caption). While Fig. 3(b) shows the results for 10 mm ID pipe in the horizontal orientation. In horizontal case, dry-out is observed at about 80 W of heat input, as seen in Fig. 3(b), characterized by a sudden rise in the evaporator section temperature. It can also be noted that the thermal resistance between the condenser-evaporator sections shows a decreasing trend. This trend is observed because, at low heat input, the average temperature of the condenser is nearly equal to the coolant temperature as the whole length of the condenser is not needed to reject heat (at low power input). As power input is increased, the average condenser temperature rises and hence thermal resistance decreases.

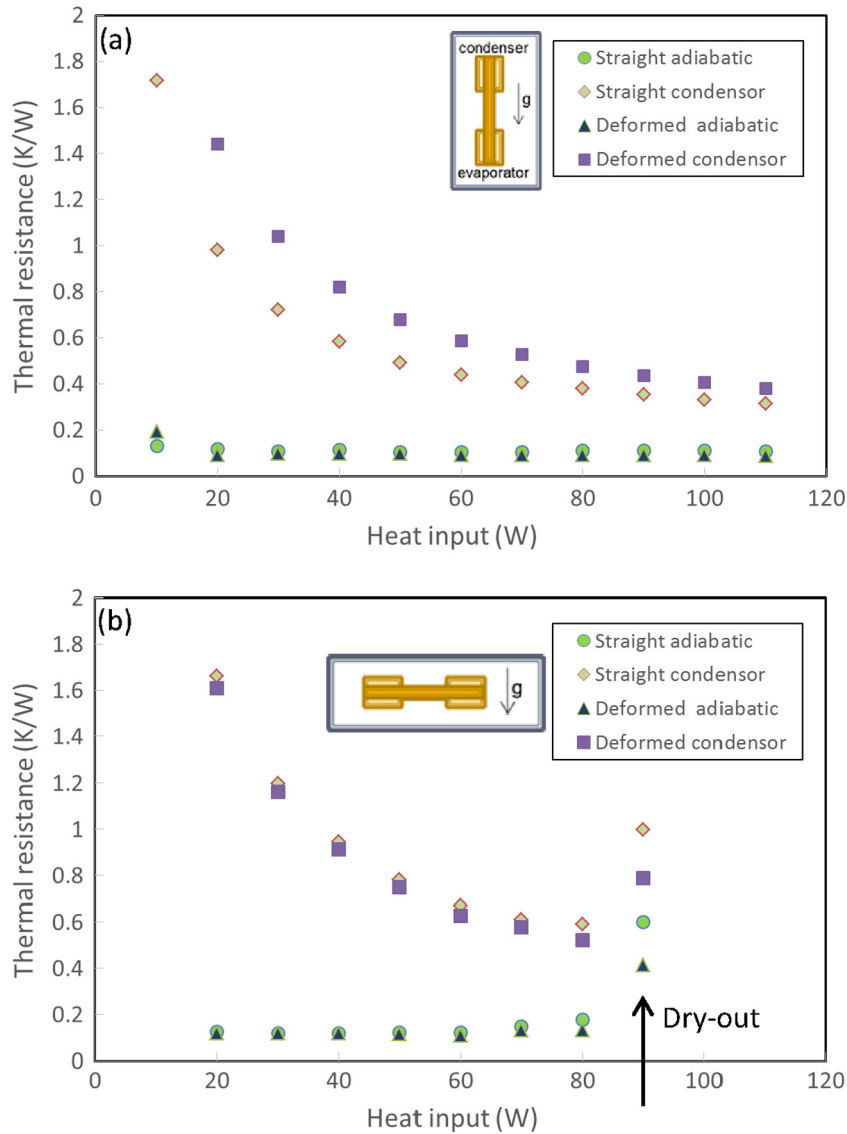


Fig. 3. Thermal resistance 10 mm ID heat pipe ($L_t = 270$ mm; $L_{adb} = 130$ mm; $L_{cond} = 70$ mm; $L_{evp} = 70$ mm; $L_{eff} = 200$ mm) at coolant temperature of 25 °C in both straight and deformed configurations for (a) vertical (heater down) positioning of the heat pipe (b) horizontal position of the heat pipe.

4.2. Heat pipe of ID 6 mm

Fig. 4(a) shows the thermal resistance for 6 mm internal diameter heat pipe in the vertical (heater down) orientation, while Fig. 4 (b) shows the results in the horizontal orientation (the dimensions of the heat pipe are given in the caption). For this pipe, dry-out is observed in both vertical and horizontal orientations. As expected, the dry-out is earlier in horizontal orientation than in gravity assisted vertical orientation. It can also be noted that this dry-out is somewhat delayed in the deformed configuration. This could be explained by unsatisfactory contact of wick at evaporator and condenser sections of the heat pipe, which improves a little when the heat pipe is deformed (bent) since at deformed configuration some portion of the wick gets in better thermal contact with the walls of the evaporator and the condenser, thereby improving the heat transfer characteristics.

As apparent from the results above, this heat pipe (6 mm ID) requires further improvement at the stage of integration of wick structure with the pipe wall, to perform still better thermally and avoid dry-outs in the operating range of temperatures.

4.3. Mechanical testing of bellow

The bellows, used in the heat pipes to provide required flexibility, were tested for the deformations that they will undergo when subjected to internal and external loads. Fig. 5(a) shows the expansion in the axial direction of bellow and Fig. 5(b) shows expansion in the radial direction. The bellow used in this experiment has 6 mm ID and length 50 mm. The deformation is measured experimentally using laser sensors, as internal hydrostatic pressure is varied from 1 bar to 25 bars.

To check the bellow for static deformations, the internal pressure is increased in small steps using a hydraulic pump. Plastic behavior of the bellow material can be clearly observed in Fig. 5 (the FEM simulation results shown in this figure will be discussed later); there is some visible permanent deformation after applied pressure is slowly reduced. The bellow withstood the pressure of ~25 bars. This range of pressure is likely to occur in the system if another fluid, e.g., ammonia is used as the working fluid, say for space thermal management application. The maximum expansion in the axial direction is less than 0.15 mm and that in the

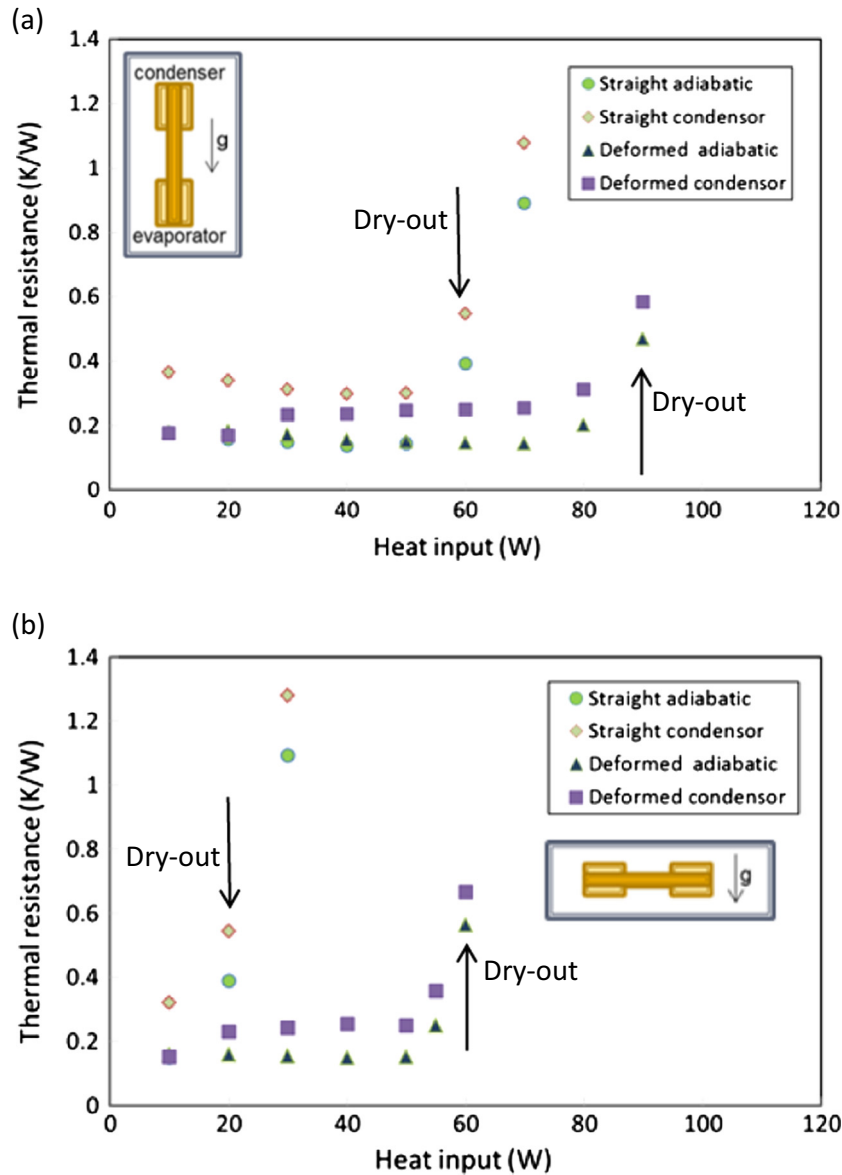


Fig. 4. Thermal resistance 6 mm ID heat pipe ($L_t = 270$ mm; $L_{adb} = 130$ mm; $L_{cond} = 70$ mm; $L_{evp} = 70$ mm; $L_{eff} = 200$ mm) at coolant temperature of 25 °C in both straight and deformed configurations for (a) vertical (heater down) positioning of the heat pipe (b) horizontal positioning of the heat pipe.

radial direction is less than 0.07 mm. In Fig. 6, net strain of the bellow, in radial and axial direction as defined below, is plotted as a function of hydrostatic pressure.

$$\epsilon_{axial} = \frac{\Delta L}{L} \quad (3)$$

$$\epsilon_{radial} = \frac{\Delta r}{r} \quad (4)$$

As per EJMA standards, the axial stiffness is defined as:

$$K_{axial} = \frac{\pi}{2(1-\nu^2)} \left(ED_m \left(\frac{h}{w} \right)^3 \left(\frac{n_p}{N} \right) \right) \frac{1}{C_f} \quad (5)$$

Here, C_f is the design coefficient which is evaluated based on C_1 , C_2 , defined as:

$$C_1 = \frac{p}{2w}; \quad C_2 = \frac{p}{2.2\sqrt{D_m h}}$$

The variation of C_f with C_1 , C_2 is given in ASME standards [15]. In addition, for a given angular deflection (θ), the angular moment on the bellow is given as:

$$M_\theta = \frac{K_{axial} D_m^2 \theta}{8}$$

Since, in our experimental test case, we have used a tip loading condition instead of a pure moment, therefore, $M_\theta = F_\theta l$, where, F_θ is the applied tip load. Further, for small bending deflections as in the present case, $\theta = y/l$, where y is tip deflection. Hence, the angular stiffness of the bellow is given by:

$$K_\theta = \frac{K_{axial} D_m^2}{8l^2} \quad (6)$$

As per EJMA, the above expressions are only valid in the elastic range and for bellows satisfying the condition $Np < 3D_b$, where, N is the number of convolutions, p is the pitch of the bellow, and D_b is

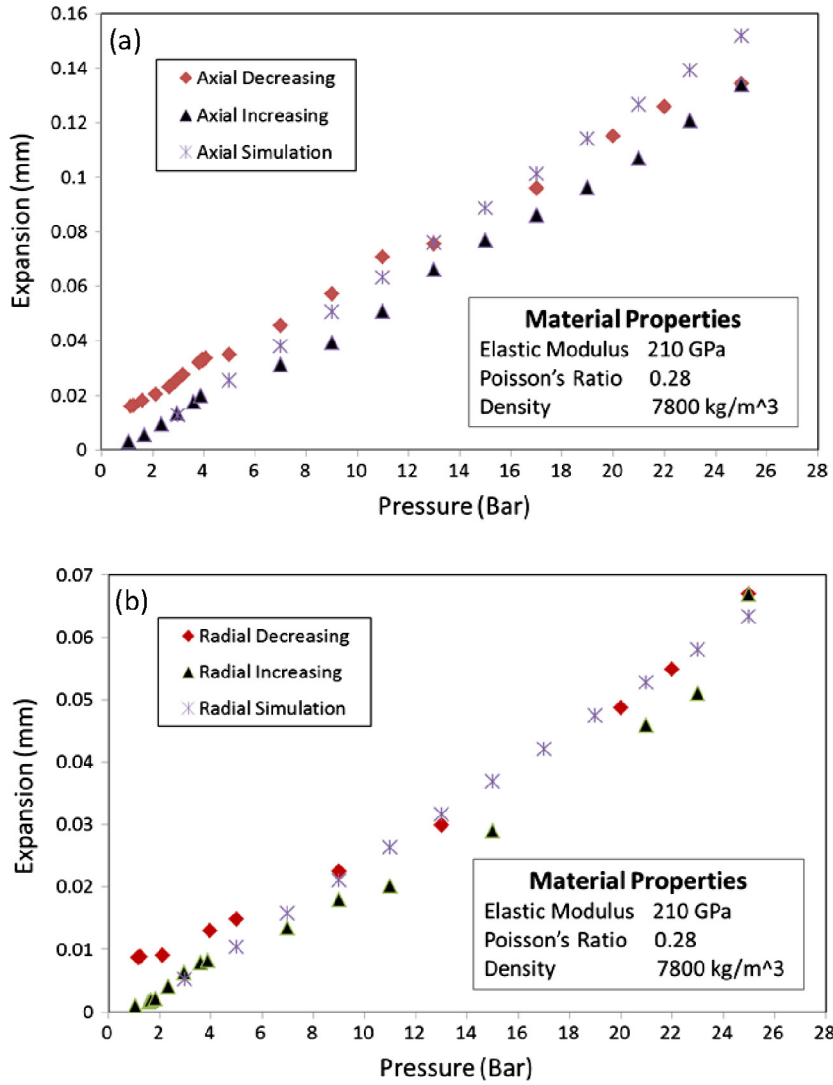


Fig. 5. Pressure v/s expansion of bellow when the pressure is varied from 1 to 25 bar and back to 1 bar in (a) axial direction (b) radial direction.

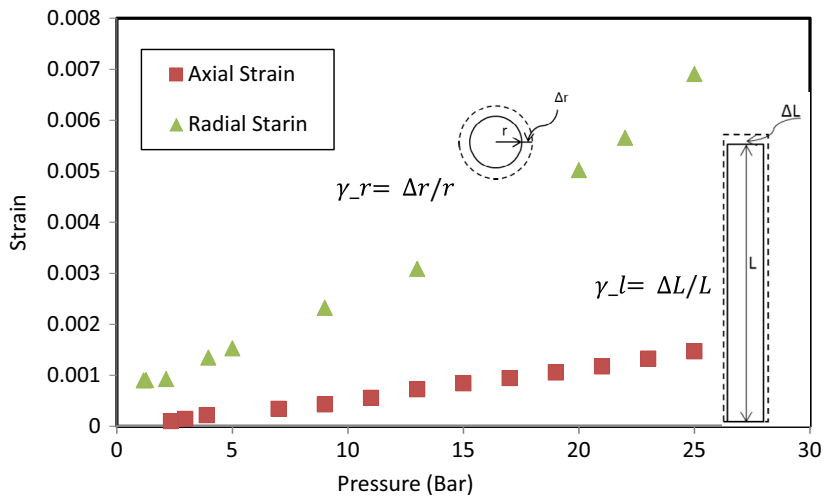


Fig. 6. Strain of the bellow under expansion due to hydrostatic pressure.

the inner diameter of the bellow. The 6 mm ID bellow does not really satisfy the above condition. However, due to non-availability of explicit EJMA standards for our test case, we have applied the above expressions, as a first approximation, to estimate the required stiffness values of the bellow. As will be seen later, the EJMA recommendations do provide a reasonable framework to estimate the required stiffness values.

The geometric profile of the bellow is shown in Fig. 7(a). Fig. 7(b) and (c) shows the bellow subjected to pure tensile load and tip load, respectively, as was done in the experiments. Using Eq. (5), theoretical axial stiffness (K_{axial}) and angular stiffness (K_{θ}), respectively, can be calculated. Fig. 8(a) shows the axial deflection v/s axial load plot, it is the same data as given in Fig. 6; only the pressure is converted to axial load by multiplying it with the inner cross section area of bellow (πr_i^2) and the axial deflection is obtained from axial strain by multiplying it with length of the bellow. Fig. 8(b) shows the bellow tip deflection v/s the applied tip load. The tip deflection is experimentally measured using the laser based displacement sensors, when the tip load is varied from 0.1 N to 1 N. The value of the axial stiffness and angular stiffness for the 6 mm bellow obtained using the EJMA standards is 407.5 N/mm and 0.85 N/mm, respectively. The corresponding experimental results in accordance with EJMA standards come out to be 403 N/mm and 0.892 N/mm, respectively. These values are vital for future work where the bellows will be subjected to dynamic loading and pre-defined vibratory loads. The insets in Fig. 8, show the X-ray tomographic image of the bellow (as seen at the centerline transverse plane), from

which the actual geometrical dimensions, as mentioned therein, have been determined.

5. FEM simulations

Stress and deformation modeling of the metallic bellow is also performed by using the Finite Element Method (FEM) on Solidworks® platform. The material properties are considered to be isotropic and a linear elastic model is considered. A through grid independence study is carried out for four different types of mesh geometries for the bellow; accordingly the bellow is meshed with over 30,000 grid elements. The 3D model with bellow and the heat pipe container is meshed with over 50,000 grid elements. The resulting deformation of the bellow to applied internal pressure is benchmarked against the experimental results, as shown earlier in Fig. 5, wherein the axial and radial deformations are simulated for different internally applied hydrostatic pressures. As can be seen, the model satisfactorily captures the bellow behavior. Higher internal pressures are used to simulate scenarios where a different working fluid may be employed in the future. Further, to simulate the bellow under different boundary conditions, as may be experienced by it under real-time heat pipe applications, specific simulations have also been conducted, as reported next.

5.1. Simulating the bellow element

The deformations obtained by the FEM model are compared against experiments, as was earlier discussed in Section 4.3.

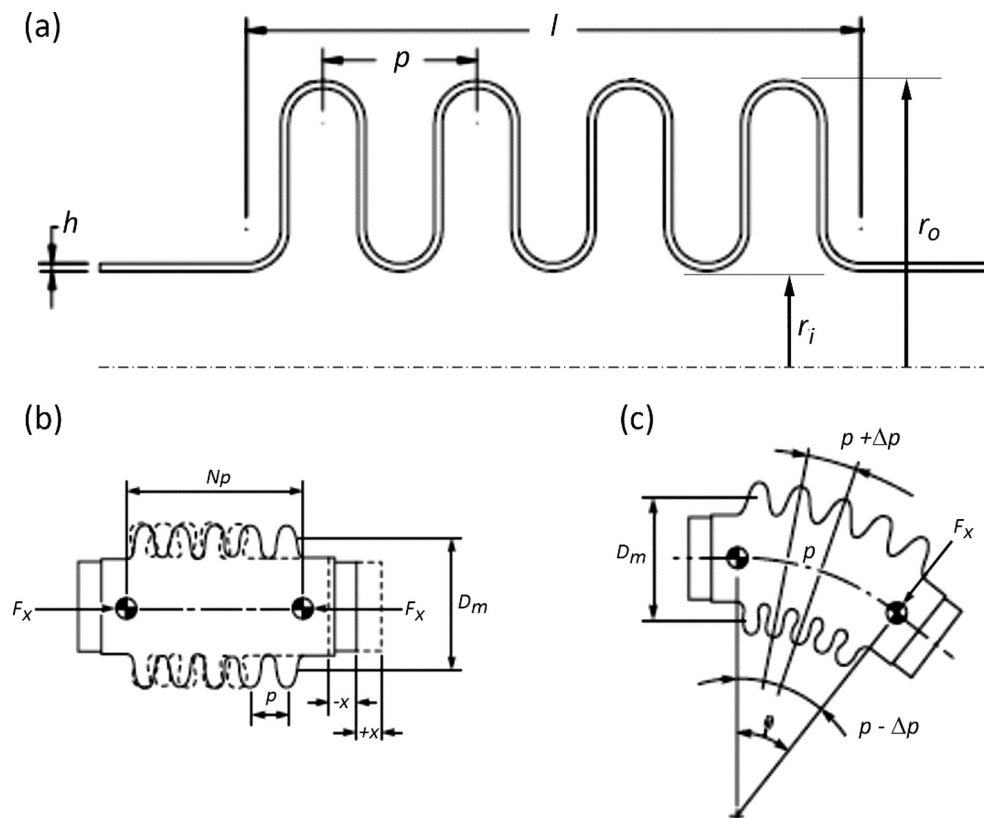


Fig. 7. Geometric profile of the bellow (a) shows the basic profile of the bellow with important dimensions (b) shows the bellow subjected to a pure tensile load F_x (c) shows the bellow subjected to a tip load F_{θ} [15].

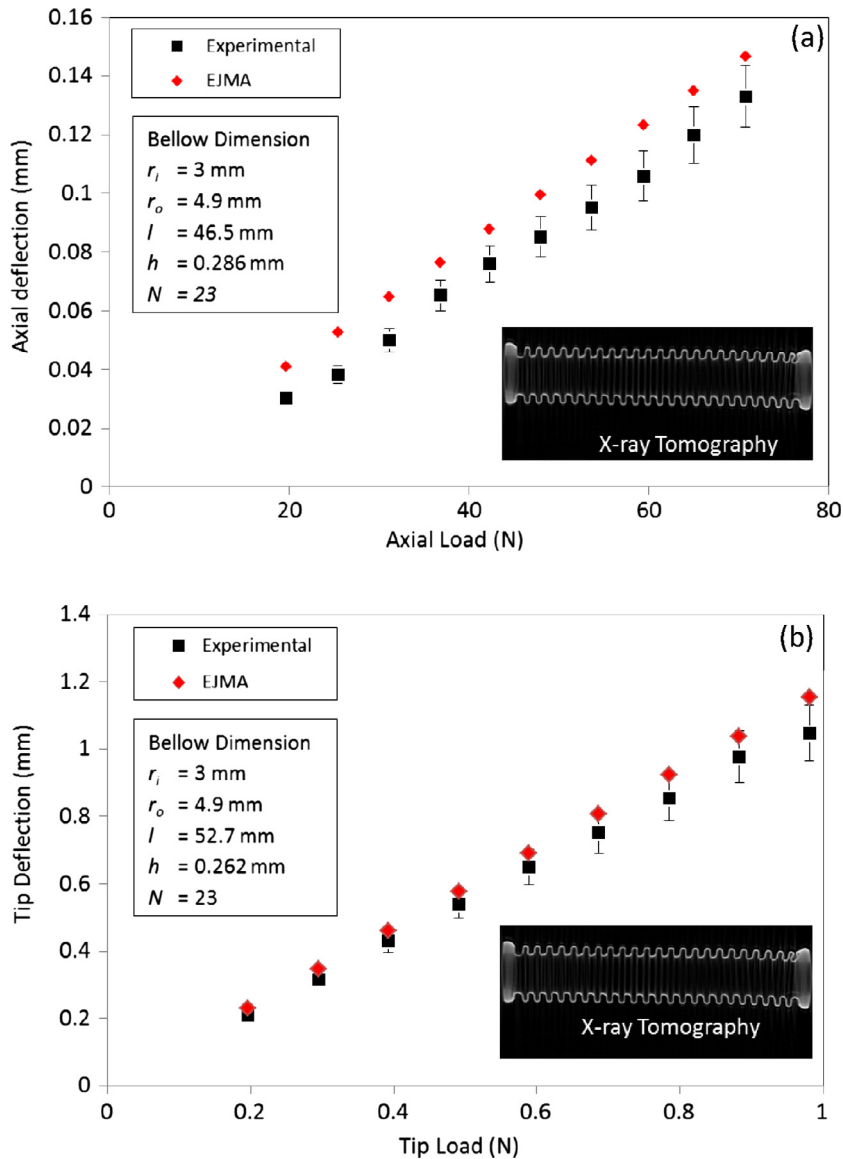


Fig. 8. (a) Axial deflection v/s axial load (data is same as depicted in Fig. 6, here internal pressure is converted to axial load by multiplying it with internal area of the bellow (πr_i^2)); (b) tip deflection v/s tip load is plotted for loads varying from 0.2 to 1 N.

Further, the model is used to determine the location of maximum stress and deformation that is occurring in the bellow, at different applied internal pressures.

Fig. 9(a) shows the total deformation of the 6 mm bellow (that is vector sum of radial and axial deformation) as obtained from the FEM model, when the bellow is clamped at one end. Fig. 9(b) shows the cross-section view of von Mises stress generated in the bellow at the applied pressure of 25 bars. Maximum von Mises stress of 290 MPa is observed at the inner tip of the bellow section at 25 bars. It may be noted that yield strength of stainless steel is 220 MPa which is lower than the maximum stress generated at 25 bars. This results in plastic deformation, as observed in the experimental results shown in Fig. 5. As the FEM model which has been used is based on linear elastic theory with isotropic material, a slight deviation from experimental data is observed for higher pressures. von Mises

stress at 17 bars is 190 MPa, as shown in Fig. 9(c). It may be inferred from the numerical study that up to about 17 bars, the bellow expands elastically, which corroborates the experimental observations.

Fig. 10 shows highly magnified expansion/deformation and stress in the bellow when both ends are fixed (clamped) and an internal pressure of 25 bars is applied. The bellow expands in radial direction and gets bent (less than $0.88 \mu\text{m}$) as the two ends are fixed. The geometry of the bellow is identical as the above modeled geometry, which is already benchmarked against the experimental results. The maximum total deformation in this case is less than $1 \mu\text{m}$ (much less than one end clamped case) as the bellow is constrained to move in the axial direction and the stress generated is only due to the pressure acting in the radial direction, the maximum von Mises stress generated being about 34 MPa.

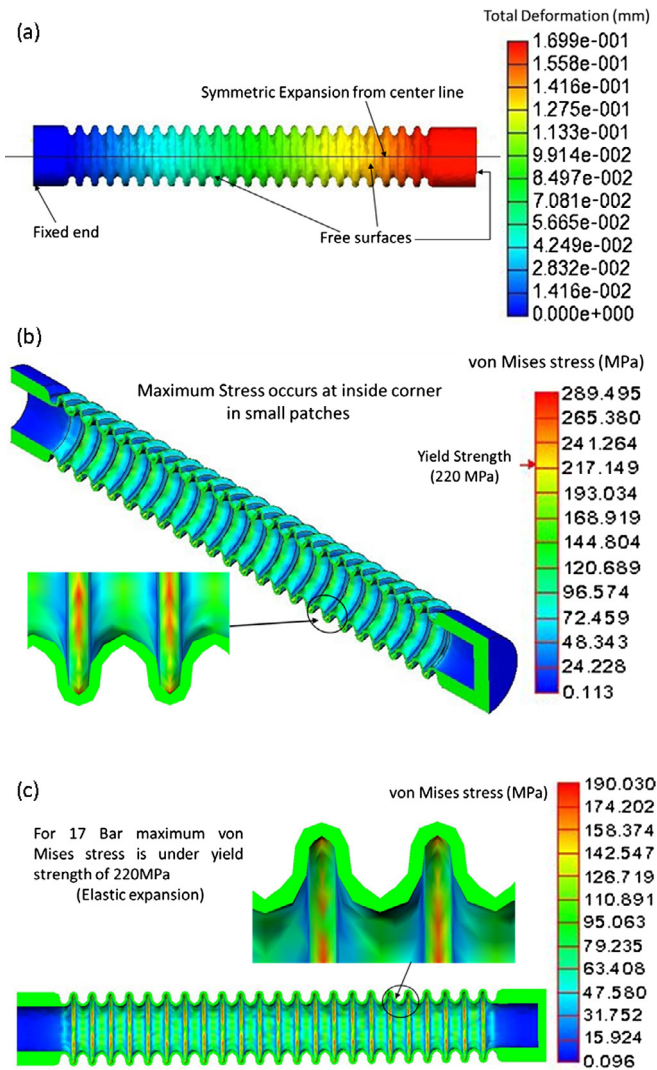


Fig. 9. Simulation results. (a) Deformed shape of the bellow with left end fix at 25 bar (Total deformation) (b) Isometric cross-section view of von Mises stress generated in the bellow at 25 bars (c) von Mises stress in the bellow at 17 bars cross-section view.

5.2. Heat pipe model with bellow element clamped at both sides

Extending the above developed model to simulate the stresses and deformations occurring in a heat pipe under clamped conditions, another finite element method (FEM) model of complete heat pipe (including two pipes attached to adiabatic bellow element) is developed in Solidworks®. This model is then subjected to different internal hydrostatic pressure, same as in the bellow model. Fig. 11(a) shows the scaled (highly magnified) deformation of the heat pipe at internal pressure of 25 bars. It may be noted that the pipe has deformed and bent slightly (1.5 μm) in the bellow section to accommodate the increased pressure. Fig. 11(b) shows cross-sectional view of von Mises stress generated in the process at 25 bars and Fig. 11(c) shows isometric view of stress generated at 17 bars. From the simulation results, it may be noted that the level of stress generated (43 MPa) is well below yield strength (220 MPa) of stainless steel at internal pressure of

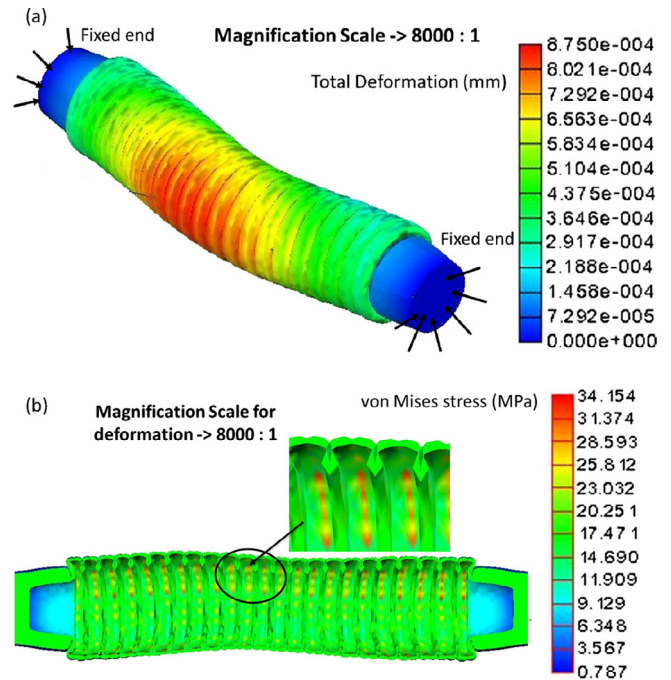


Fig. 10. Simulation results for bellow model with both ends clamped (fixed) and the internal pressure of 25 bars (a) magnified isometric view of the total deformation in the bellow (b) von Mises stress generated in the bellow (cross-section view).

25 bars. Hence, the bellow not only withstands the pressure, it also accommodates the change in length due to its expansion properties.

6. Summary and conclusions

Conventional wicked heat pipes, incorporating flexible bellows as part of the container, are developed and initial results for thermal performance and mechanical stress behavior have been reported here. Such heat pipes are needed in many applications for vibration isolation and stress-free operation. Successful operation of such flexible heat pipes has been obtained for handling about 80 W for 10 mm ID heat pipes in horizontal orientation. For 6 mm heat pipes, dry-out occurs early in horizontal operation and needs to be addressed to meet the target specifications of 60 W.

Axial and radial deformation of bellow (6 mm ID) under hydrostatic pressure up to 25 bars is under 0.15 mm and some plastic behavior is also observed as pressure is slowly decreased from 25 bars to 1 bar. A finite element (FEM) linear elasticity model is developed and is benchmarked against experiments. It is used to obtain maximum stress occurring in the bellow section subjected to internal static pressure. Variation in expansion/deformation due to change in Poisson's ratio is also noted. The axial and angular stiffness is experimentally determined and obtained values are satisfactorily compared with predictions as per design guidelines of EJMA. The studies are ongoing and the thermo-mechanical characterization of the developed heat pipes will next be undertaken under dynamic loads and specified vibration signatures expected under real-time operations.

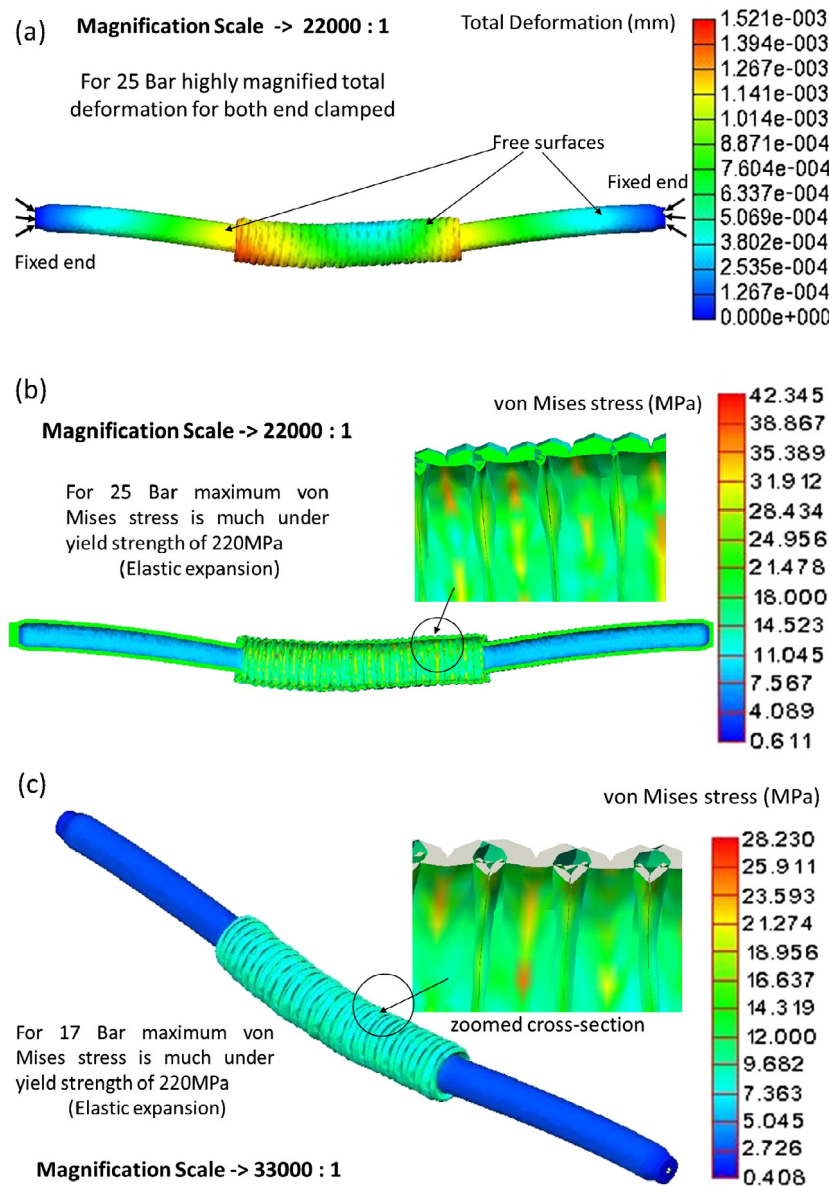


Fig. 11. Simulation results (a) deformed shape of bellow with both end fix at 25 bar (total deformation) (b) Cross-section view of von Mises stress in the bellow at 25 bars cross-section view (c) isometric cross-section view of von Mises stress generated in the bellow at 17 bars.

Acknowledgements

Research funding is provided by ISRO (Indian Space and Research Organization) via the Space Technology Cell, IIT Kanpur, India. We thank Mr. Lakshya Gangwar (internship student under the Summer Undergraduate Research and Graduate Excellence program of IIT Kanpur, 2016) and Mr. Ravi Sharma (Graduate student, IIT Kanpur) for their assistance.

References

- [1] P.D. Dunn, D.A. Reay, *Heat Pipes*, Pergamon Press, Oxford, 1976.
- [2] A. Faghri, *Heat Pipe Science and Technology*, Taylor & Francis, 1995.
- [3] S.W. Chi, *Heat Pipe Theory and Practice*, a Sourcebook, Hemisphere Publishing Corporation, 1976.
- [4] Q. Lü, J. Hu, D. Cheng, J. Liu, Y. Jiang, Experimental study of airborne heat pipe cold plate under vibration and acceleration conditions, *Nanjing Hangkong Hangtian Daxue Xuebao/J. Nanjing Univ. Aeronaut. Astronaut.* 46 (2) (2014) 316–321.
- [5] A. Alaei, M.H. Kafshgari, S.K. Rahimi, A vertical heat pipe: an experimental and statistical study of the thermal performance in the presence of low-frequency vibrations, *Heat and Mass Transfer/Waerme- und Stoffuebertragung* 49 (2) (2013) 285–290.
- [6] R.-H. Chen, Y.-J. Lin, C.-M. Lai, The influence of horizontal longitudinal vibrations and the condensation section temperature on the heat transfer performance of a heat pipe, *Heat Transfer Eng.* 34 (1) (2013) 45–53.
- [7] H.-U. Oh, Performance investigation of spaceborne micro-vibration isolation system combined with heat pipe cooling system, *Proceedings of the International Astronautical Congress, IAC 7* (2011) 5680–5686.
- [8] S.-S. Hsieh, Y.-R. Yang, Design, fabrication and performance tests for a polymer-based flexible flat heat pipe, *Energy Convers. Manage.* 70 (2013) 10–19.
- [9] C. Yang, S. Song, W. Shang, P. Tao, D. Tao, Flexible heat pipes with integrated bioinspired design, *Progress Natural Sci.: Mater. Int.* 25 (1) (2015) 51–57.
- [10] J.A. Haringx, Instability of bellows subjected to internal pressure, *Philips Res. Rep.* 7 (3) (1952).
- [11] H. Reissner, Über die unsymmetrische Biegung dünner Kreisringplatten, *Ing. Archiv* 1 (1929) 72.
- [12] D.E. Newland, Buckling of double bellows expansion joints under internal pressure, *J. Mech. Eng. Sci.* 6 (3) (1964).
- [13] I.V. Meyer, Heat pipe with a flexible structure, United States Patent Pub. No.: US2011/0088874, 2011.
- [14] Huang, Flexible heat pipe and manufacturing method thereof, United States Patent Pub. No.: US2011/0220328, 2011.
- [15] ASME Boiler and Pressure Vessel Code 2010, VIII Division 1 Rules for Construction of Pressure Vessels, 978–0, ISBN no-7918-3251-6, New York, 530–554.